Wave Inversion Technology, Report No. 2, pages 57-66

Prestack Kirchhoff depth migration with dynamic wavefronts applied to SEG/EAGE Salt dataset

L. Pasasa, F. Wenzel, and P. Zhao[1]

keywords: *Imaging, Wavefronts, Traveltimes, Salt*

ABSTRACT

Prestack Kirchhoff depth migration using dynamic wavefronts Pasasa et al. (1997a) is applied to the slice A-A' of SEG/EAGE Salt dataset to test the accuracy and stability of the method. The migrated image created using dynamic wavefronts is superior to one created using Fermat wavefronts. Not only most of the subsalt structure is clearly imaged, but also the near vertical reflectors, including steeply dipping interfaces and reflecting faults which are missing in the Fermat image, are correctly imaged.

INTRODUCTION

Imaging of subsalt structures is important for oil and gas exploration in some areas, such as the Gulf of Mexico and North Sea. The recently developed SEG/EAGE Salt model O' Brien and Gray (1996) and the related synthetic data presents technical challenges to imaging methods. Strong velocity contrasts between the salt body and the surrounding medium, irregular surfaces of the salt body, steep salt flanks and steep faults, are causing difficulties in subsalt imaging when using Fermat wavefronts in prestack Kirchhoff migration. In complex velocity fields, Fermat wavefronts may be non-energetic energy headwaves and are thus inappropriate for use in migration.

The traveltime field in complex velocity media is generally a multi-valued function of subsurface positions because of possible multiple arrivals. Whereas some arrivals are identifiable by kinematic properties of seismic waves (Fermat wavefronts), others have to be identified by dynamic properties (dynamic wavefronts) Pasasa et al. (1997a) which are consistent with the dominant (energetic) events in the data. The energy carried by Fermat wavefronts may become considerably weaker than that carried by dynamic wavefronts. In such situations, dynamic wavefronts are needed in order to maximize the imaging capability of Kirchhoff migration.

[1]**email:** lpasasa@gpiwap5.physik.uni-karlsruhe.de

We applied prestack Kirchhoff depth migration using dynamic wavefronts to the slice A-A' of SEG/EAGE Salt dataset and show that a superior image can be achieved that contain not just subtle improvements but a qualitative step forward in resolution and signal-to-noise ratio.

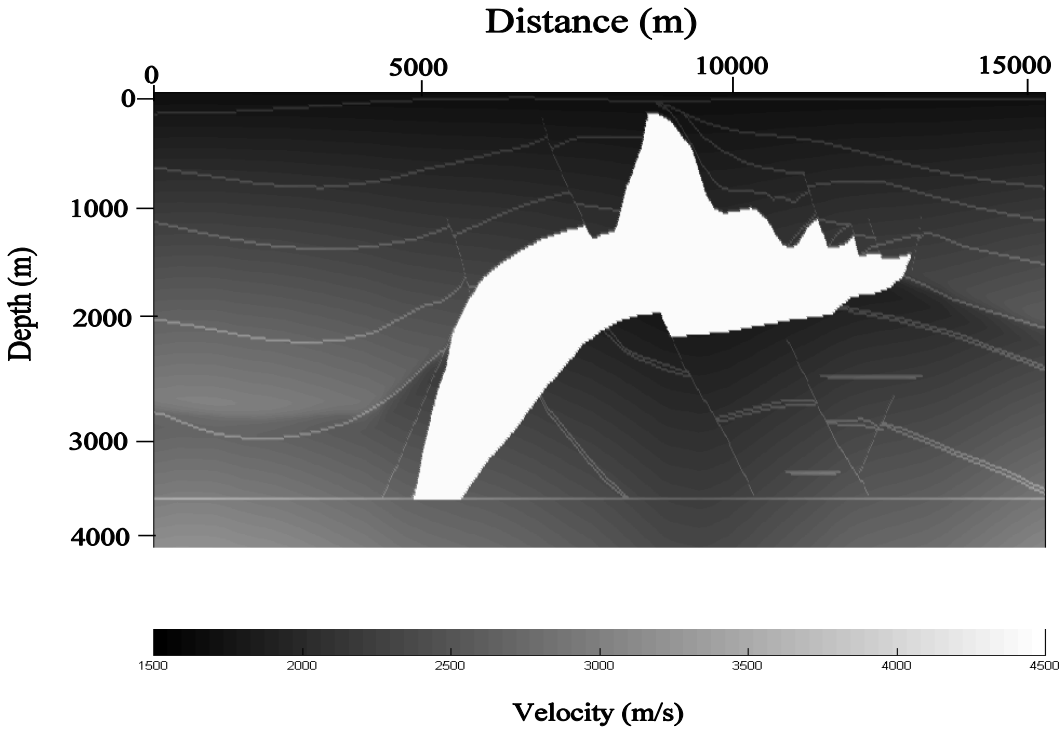

Figure 1: Profile A-A' of the SEG/EAGE Salt dome model crosses many of the more difficult structural elements in the model.

BRIEF DESCRIPTION OF TRAVELTIME CALCULATION

Traveltime calculation is a crucial part of prestack Kirchhoff migration schemes. Pasasa et al. (**?**) present an effective method to calculate the maximum energy traveltimes. Our new criterion is to modify the traveltime calculation that does not comply with Fermat's principle of least times. By ignoring the contribution of the refracted waves, we are able to calculate wavefronts which are consistent with the dominant (energetic) events in the data. The output wavefronts, which we name dynamic wavefronts, can then be used for Kirchhoff migration. This method has the following properties:

- The dynamic wavefront criterion generally tracks a high amplitude arrival.
- It almost never chooses a low amplitude Fermat wavefront associated with refracted energy in a complex velocity environment.

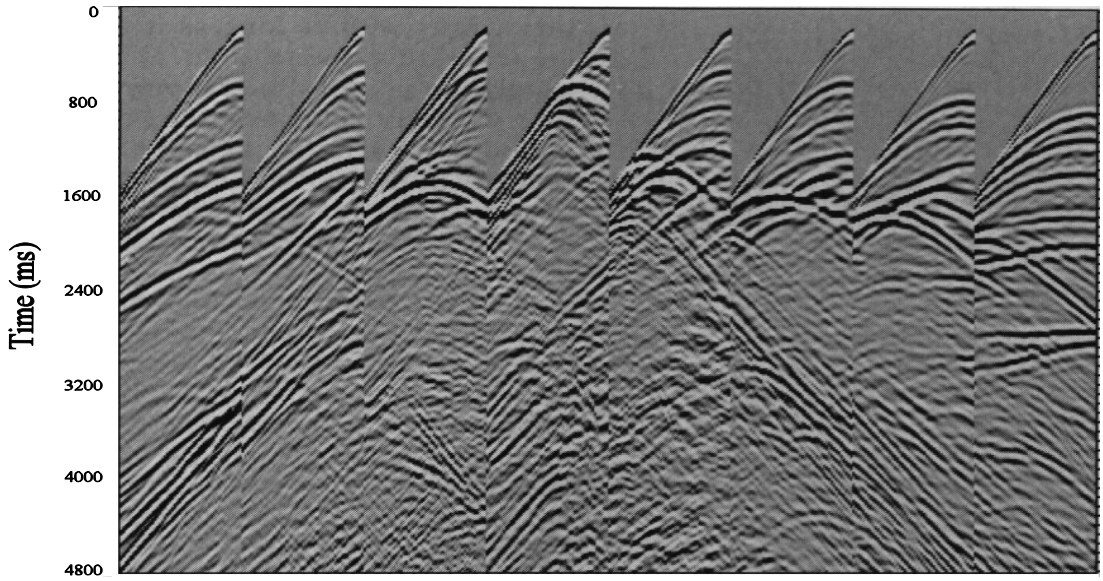

Figure 2: Several synthetic shot records acquired across the model, with free surface multiples suppressed.

- Since the wavefront can be calculated in any velocity model, there is no smoothness constraint.
- It is much more stable with respect to irregularities or changes in the velocity model.
- It performs even better computationally than Fermat wavefront calculation.

DESCRIPTION OF THE SEG/EAGE SALT DATASET

A 2-D profile (slice A-A′) of the SEG/EAGE Salt model (Figure 1), which crosses many of the difficult structural elements in the model, steep, shallow salt flanks, divergence between the top and base of salt, and abrupt dip changes where the faults are located, poses challenges to the imaging methods.

The synthetic seismic data consist of 325 shot records with 174 traces per shot moving from left to right through the model. The first shot is at x=0, and the receiver line belonging to this first shot starts at x=-4267 m and ends at x=0. The shot interval is 48.8 m, the receiver interval is 24.4 m. Record length was 4800 ms with a 8 ms sample rate and the maximum frequency present in the data is about 25 Hz. The dataset does not have the surface-related multiples. Figure 2 shows several shot records from the synthetic dataset. The shots contain complicated non-hyperbolic moveout and backscattered energy.

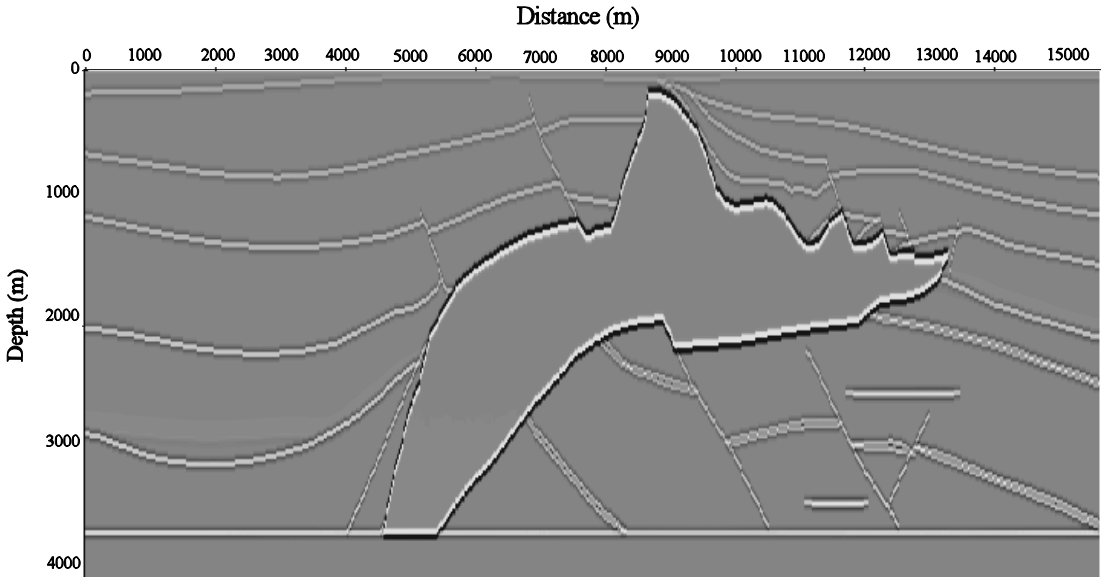

Figure 3: Synthetic reflectivity section for profile A-A' of the SEG/EAGE Salt model. This section is obtained by combining the velocity and density models and convolving with a wavelet.

Since the SEG/EAGE Salt model is synthetic, the image can be compared with the velocity model to determine the accuracy of the migration algorithm. Figure 3 shows a synthetic reflectivity section. The velocity and density models were combined and then convolved with a wavelet to produce this section. This type of resolution cannot be expected from migration, but ideally, the migration results should provide a comparable structural image.

Figure 4 shows contour traveltimes superimposed on the velocity model. The point source is situated at the surface (x=6200 m). The solid curve represents Fermat wavefronts and the dashed curve stands for dynamic wavefronts. Comparing these dynamic wavefronts with Fermat wavefronts, we generally see good agreement in the sediment layers and steeply dipping near-surface faults. However, the rugose top of salt has created refracted arrivals through the salt that carry little energy at the bottom salt. The steep subsalt structures are similarly affected.

Figure 5 displays the distribution of relative delay between Fermat wavefront and dynamic wavefront. Figure 6 shows the curves of relative delay at offset x=6000 m, 7000 m, and 12000 m. There is no delay in the sediment layers. The relative delay, however, is larger than -4 percent in the subsalt structures, where the difference between direct waves and head waves in the model becomes apparent.

The maximum misfit of approximately 4.5 wavelength between Fermat wavefront and dynamic wavefront is caused by refractions. Based on the criterion, that two seis-

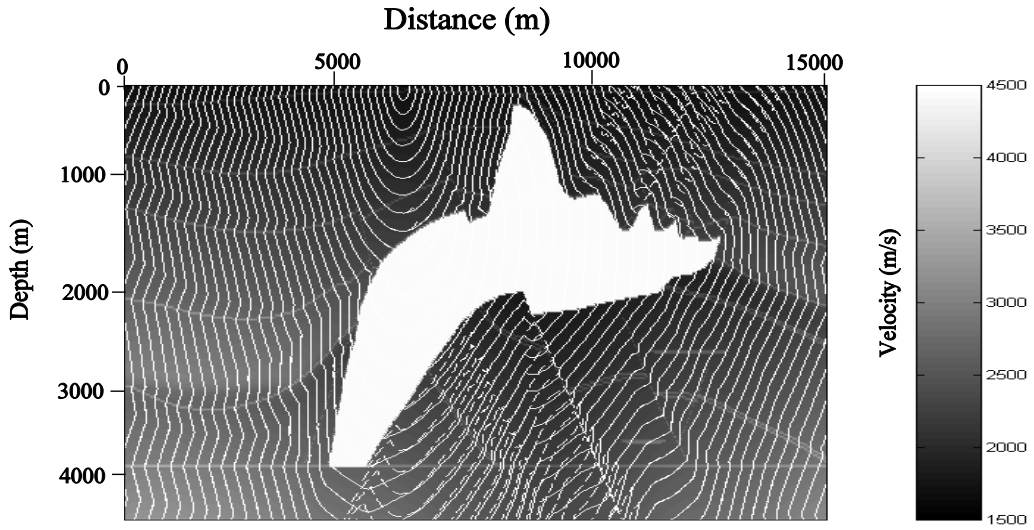

Figure 4: Traveltime contours of the SEG/EAGE Salt model caused by a point source placed on the surface at x=6200 m. The large difference of approximately 4.5 wavelength between Fermat wavefront (solid curve) and dynamic wavefront (dashed curve) is caused by refractions.

mic events can be resolved if they are separated at least by a half wavelength, this misfit can cause a significant difference image result in the subsalt structure between migration using Fermat wavefront and dynamic wavefront. The result is verified in Figure 7, which shows the result of finite difference wave-equation modeling. The figure displays a snapshot of the wavefield at time 2 s. It represents the full two-way Green's function at 2 s. The waveform source is a 25 Hz wavelet. The dynamic wavefront is a much closer fit to the major events in the full Green's function. We note here that the comparison with the wavefield confirms the accuracy of the method in calculating larger energy traveltimes.

IMAGING WITH FERMAT WAVEFRONT

The result of prestack Kirchhoff depth migration using Fermat wavefronts is shown in Figure 8. We use the true velocity model; no smoothing was done. It does a fairly good job for this difficult case. Most of the top of salt structures are imaged quite well. However, the sudden dip changes in the top of salt caused significant diffractions at the bottom of the salt. Since the method used Fermat wavefronts, it seems that the rugose top of salt has created refracted arrivals through the salt that carry little energy at the bottom salt. The steep subsalt structures are similarly affected. Reflecting fault planes at points A and B, as well as the dipping reflector at point C are not well

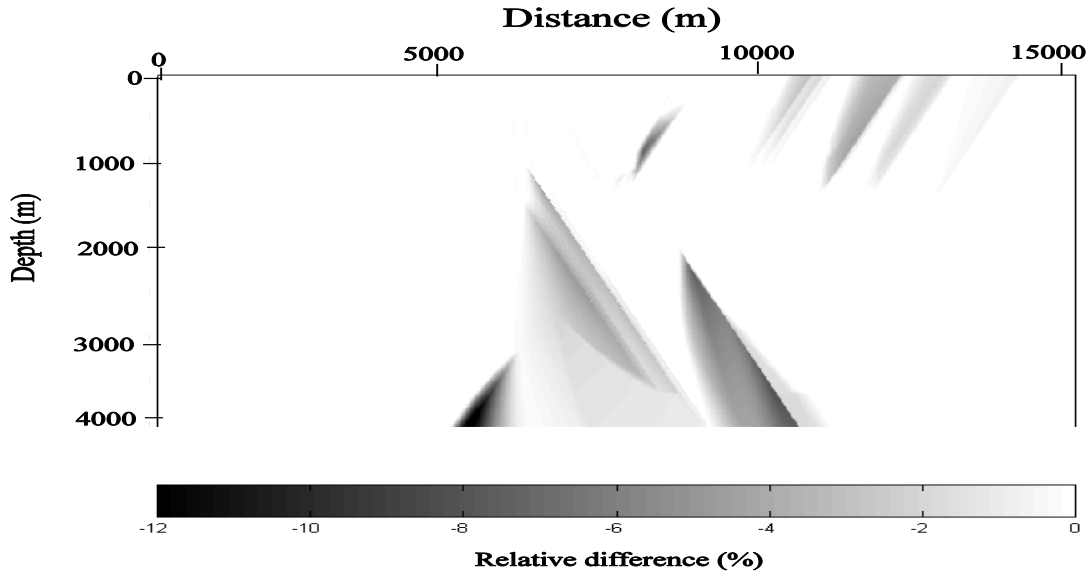

Figure 5: Relative difference between Fermat wavefront and dynamic wavefront. Values range from -12 % to 0 %.

imaged or missing. Coherent noise from incorrectly migrated fields are strong under the salt body. Furthermore, some false faults appeared due to the possible interference of coherent noise phases, such as a false fault on the left of the fault B is presented but the fault itself is missing. Despite this, migration with the Fermat wavefronts was able to image the sediment layers and steeply dipping near-surface faults.

IMAGING WITH DYNAMIC WAVEFRONT

The result of prestack Kirchhoff depth migration using dynamic wavefronts is shown in Figure 9. Improvements can be seen when it is compared to the one obtained by using Fermat wavefronts, particularly under the rugose top of salt. Not only most of the subsalt structure is reconstructed clearly, but also the near vertical reflectors, including steeply dipping interfaces and reflecting faults, some of which are missing even in the Fermat image, are correctly imaged. Reflectors A, B and C, all showed up. Especially the fault B appeared clearly and in the correct position. Because of the accurate image of the fault B, the coherent noise around that fault is much reduced and therefore the curved reflecting interface between B and C is also correctly imaged. This demonstrates the applicability of the Kirchhoff migration method using dynamic wavefronts to subsalt structured imaging and structured imaging in other strong-contrast complex situations.

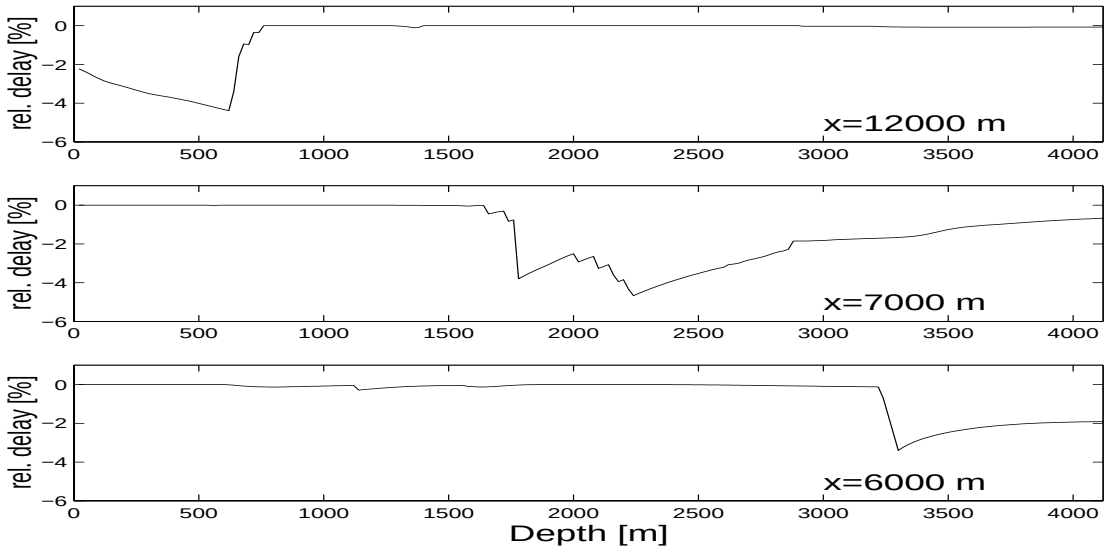

Figure 6: Plot of relative delays corresponding to traveltimes of Figure 4 at offset x=6000 m, 7000 m and 12000 m.

SUMMARY

Prestack Kirchhoff depth migration with dynamic wavefronts is tested using the slice A-A' of SEG/EAGE Salt dataset. The migrated image created using dynamic wavefronts is superior to one created using Fermat wavefronts. Not only most of the subsalt structure is clearly imaged, but also the near vertical reflectors, including steeply dipping interfaces and reflecting faults which are missing in the Fermat image, are correctly imaged. The Fermat image missed almost all the near vertical subsalt structures and has distorted images especially for flat subsalt interfaces. The dynamic image has much less migration noise than the Fermat image. This demonstrates the applicability of the Kirchhoff migration method using dynamic wavefronts to mapping subsalt structure.

REFERENCES

O' Brien, M. J., and Gray, S. H., 1996, Can we image beneath salt?: The Leading Edge, **45**, 17–22.

Pasasa, L., Wenzel, F., and Zhao, P., 1997a, Imaging complex 2D structure with non-Fermat arrival Kirchhoff depth migration: 1st Ann. Report, Wave Inversion Technology, No. 1, 97–104.

Pasasa, L., Wenzel, F., and Zhao, P., 1997b, Prestack high-resolution imaging with

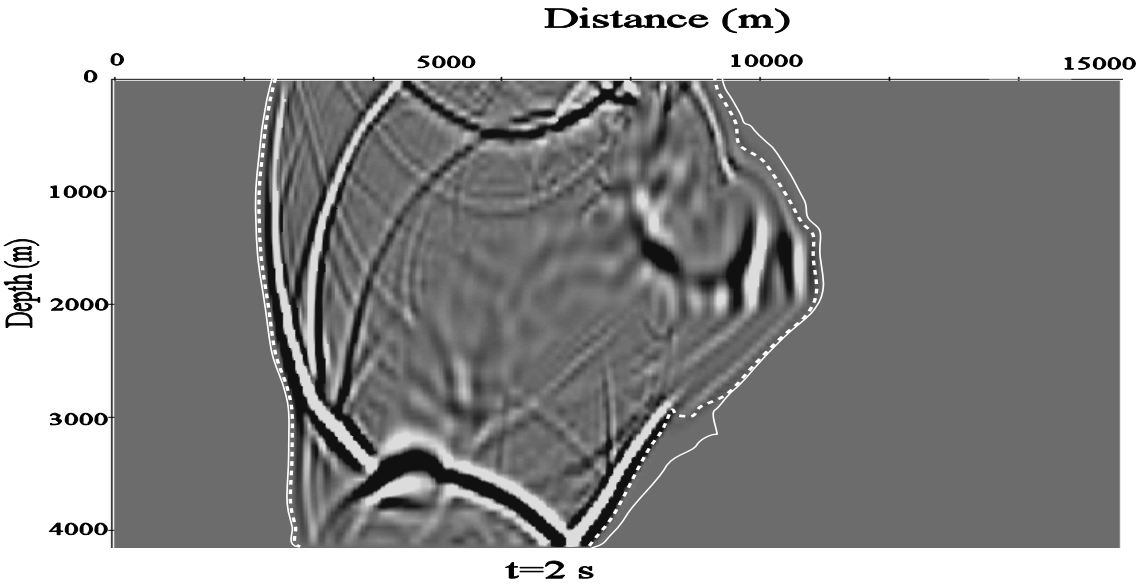

Figure 7: Acoustic wavefield modeling overlaid by contours of Fermat (solid white line) and dynamic (dashed line) wavefronts superimposed on a snapshot of the acoustic wavefield at 2 s. The point source is positioned at x=6200 m.

non-Fermat arrival traveltimes: 68th Ann. Internat. Mtg., Soc. Expl. Geophys., Expanded Abstract, Traveltimes II: Eikonal and Huygens.

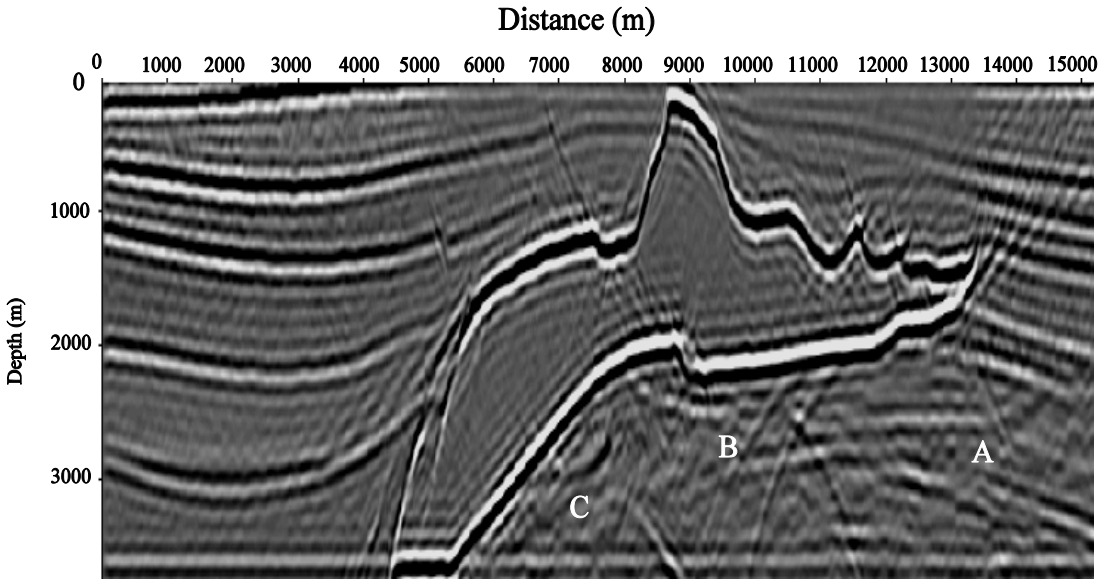

Figure 8: Imaged depth section using Fermat wavefronts. Reflecting fault planes at point A and B, as well as the steeply dipping interfaces at point C are not well reconstructed or totally missing. Coherent noise from incorrectly migrated fields are strong under the salt body.

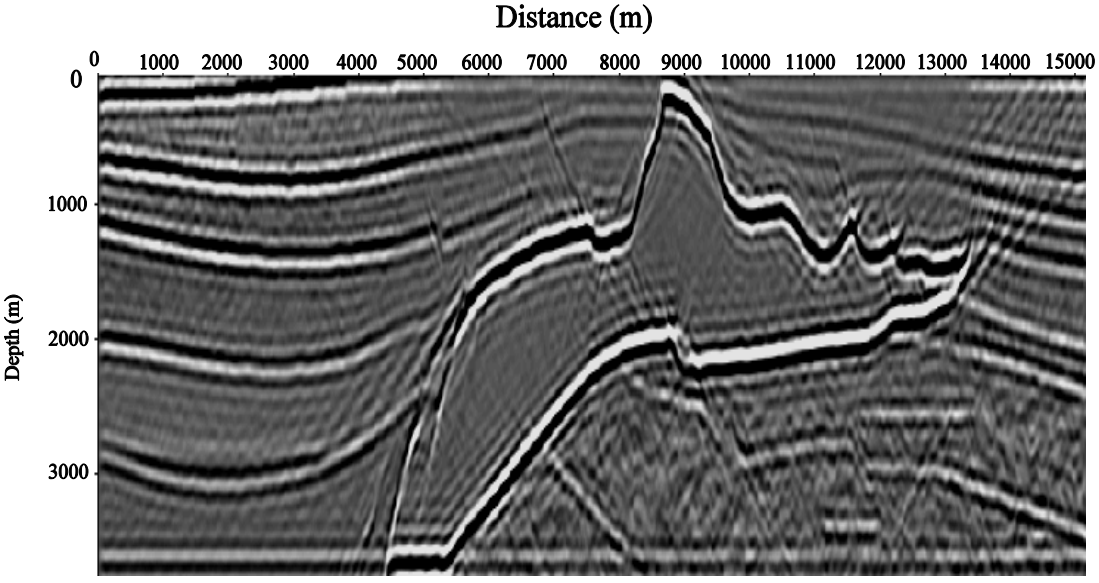

Figure 9: Imaged depth section using dynamic wavefronts. Not only most of the subsalt structure is reconstructed clearly, but also the near vertical reflectors, including steeply dipping interfaces and reflecting faults, some of which are missing even in the Fermat migrated image, are correctly imaged.